JOURNAL OF SOLID STATE CHEMISTRY 137, 168–173 (1998)
ARTICLE NO. SC987749

Study of the Conductivity of $Na_{x-\delta}Fe_xTi_{2-x}O_4$ ($x = 0.875$, $0 \leq \delta \leq 0.40$)

A. Kuhn,*,[1] C. León,† F. García-Alvarado,* J. Santamaría,† E. Morán,‡ and M. A. Alario-Franco‡

*Departamento de Química Inorgánica y Materiales, Facultad de Ciencias Experimentales y Técnicas, Universidad San Pablo – CEU, 28668 Boadilla del Monte, Madrid, Spain; †Departamento de Física Aplicada III, Facultad de Ciencias Físicas; and ‡Departamento de Química Inorgánica, Facultad de Ciencias Químicas, Universidad Complutense, 28040 Madrid, Spain

Received July 22, 1997; in revised form December 19, 1997; accepted December 23, 1997

Complex admittance measurements are performed on $Na_{x-\delta}Fe_xTi_{2-x}O_4$ ($x = 0.875$, $0 \leq \delta \leq 0.40$) polycrystalline samples, which have been prepared by the standard ceramic method and further treated by soft chemistry extraction reactions. The parent, nonextracted sample has a Na content of 0.875 ions per formula and shows a single activation energy in the dc conductivity of 1.1 eV. The conduction process is due to ion motion along the double tunnels parallel to the short *b* axes of the quadruple rutile structure. When Na is removed, a decrease in the activation energy is observed. This can be interpreted in terms of an increased ion mobility due to the increased number of vacancies created on sodium extraction. In addition, a second, less activated process, which is attributed to an electronic contribution produced by the partial oxidation of Fe^{3+} to Fe^{4+}, appears on Na removal.

1. INTRODUCTION

Chemical extraction reactions have been used, up to now, in only a few cases to modify the transport properties of solids. This is in great contrast to the inverse process, the chemical insertion reactions, which are very often used for that purpose. Several examples include the well known tungsten bronzes (1) and more recently, $YBa_2Cu_3O_7$ after lithium insertion (2). For succeeding in soft-chemistry extraction reactions, starting oxides have to fulfil some requirements, such a structure with occupied sites that can be emptied and oxidizable metallic cations possessing at least two different feasible oxidation states.

A number of quaternary oxide systems presenting the open calcium ferrite type structure (3) are known (4–6). The common structural feature of all these compounds is infinite chains formed by octahedra sharing edges that run parallel to the *b*-axis. The basic structural unit of the non-stoichiometric $Na_xFe_xTi_{2-x}O_4$ is a zigzag quadruple rutile block of edge-shared octahedra. Each zigzag block shares vertices with the next four blocks, producing large double tunnels, which are not fully occupied by sodium atoms (see Fig. 1).

Recently, we have described the partial removal of sodium from the double tunnels of $Na_xFe_xTi_{2-x}O_4$, creating further nonstoichiometry while retaining the framework structure (7). The aim of the present work is to study whether the conductivity of the starting material can be improved by partially removing sodium from the double tunnels and to analyze the concomitant changes in conductivity and sodium ion mobility, and the eventual contribution of electronic conductivity.

2. EXPERIMENTAL

The synthesis of $Na_xFe_xTi_{2-x}O_4$ ($x = 0.875$) and its oxidation were performed as previously described (5, 7).

Both the nonoxidized $Na_xFe_xTi_{2-x}O_4$ used in the oxidation reactions and the oxidized samples were checked for purity by X-ray powder diffraction methods on a Siemens D-5000 diffractometer setup with monochromated Cu$K\alpha$ radiation. Silicon was used as internal standard. A special argon-filled X-ray sample holder prevented contact with air during the X-ray experiments.

Electron diffraction experiments were done in a JEOL 2000 FX electron microscope operating at 200 kV. Specimens were prepared by grinding, dispersing in dry n-hexane, and putting a few droplets on a carbon-coated copper grid. Exposure to air only took place while mounting the grid in the sample holder.

Admittance spectroscopy measurements were conducted using an automatically controlled HP4284A precision LCR meter from 20 Hz to 1 MHz. Samples were cold-pressed into cylindrical pellets of 5 mm diameter and 0.3 mm thick, and the contacts were defined using silver paint. Samples were mounted in a sealed stainless steel holder through which high purity dry nitrogen was flown to ensure an inert atmosphere and to avoid water condensation. Temperature was varied in the range 160–600 K.

[1]To whom correspondence should be addressed.

0022-4596/98 $25.00

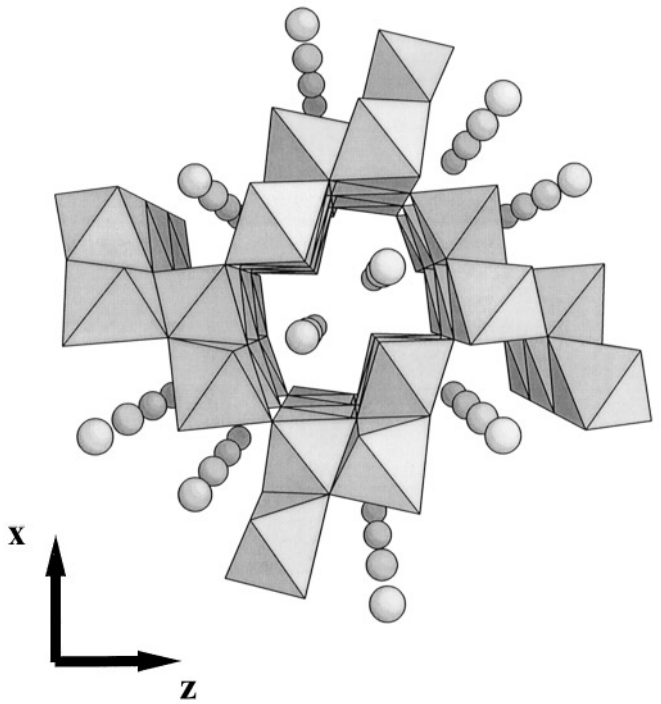

FIG. 1. Projection of the $Na_{x-\delta}Fe_xTi_{2-x}O_4$ structure along the *b*-axis. The double tunnels are perpendicular to this plane and partially occupied by sodium atoms (circles).

3. RESULTS AND DISCUSSION

3.1. Structural Characterization

The amount of extracted sodium increases with the strength of the oxidizing agent, as already shown (7). XRD patterns of the oxidized samples are very close to those of the fresh material. All the reflections of the parent compound appear for the oxidized phases indicating that the basic framework structure is maintained during the extraction procedure; no extra reflections are observed. Figure 2 shows a typical electron diffraction pattern of the parent compound taken in the [0 1 0] zone axis. The fourfold superstructure of the rutile basic cell in both the a* and c* directions can be easily recognized in all the extracted materials. Therefore, electron diffraction also shows the parent framework is kept on oxidation. We have observed that when sodium is removed, a continuous change of the cell parameters is observed. The *a*-parameter linearly increases, whereas the short *b*-parameter decreases. On the other hand, the *c*-parameter initially increases and then decreases on further extracting sodium. The combination of the different behavior of the three cell parameters causes the cell volume to remain almost unchanged. We have also recently demonstrated that after sodium extraction a slight rearrangement of the three-dimensional host structure, including the environment of the sodium atoms, takes place (8). More details about structural changes will be discussed below in light of the results obtained from complex admittance spectroscopy.

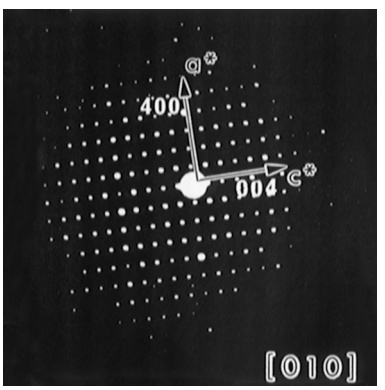

FIG. 2. Typical electron diffraction patterns of the series $Na_{x-\delta}Fe_xTi_{2-x}O_4$ taken in the [0 1 0] zone axes for a sample with $\delta = 0.40$. The fourfold superstructure of the rutile basic cell can be easily recognized.

3.2. Complex Admittance

Some of the results obtained for a sample with $\delta = 0.20$ are shown in Fig. 3. The real part of the permittivity and the real part of the conductivity are plotted vs frequency for various temperatures in Figs. 3a and 3b, respectively. A high frequency permittivity has been subtracted from the permittivity data.

The analysis of data in Fig. 3a demonstrates that the complex permittivity can be expressed using the phenomenological equation [1] proposed by Jonscher (9) as follows:

$$\varepsilon^* = \varepsilon_\infty + A(\mathrm{j}\omega)^{p-1} + B(\mathrm{j}\omega)^{n-1}, \qquad [1]$$

where ε_∞ is the high frequency permittivity, A and B are temperature-dependent amplitudes, and p and n are between 0 and 1. This behavior has been widely observed in charge carrier dominated systems, and it is believed to arise from many body interactions among moving species (9). Accordingly, the complex conductivity can be expressed as:

$$\sigma^* = \sigma_0 + \mathrm{j}\omega\varepsilon^*, \qquad [2]$$

where σ_0 is the dc conductivity.

Hence separating real and imaginary parts, the real part of the permittivity is:

$$\varepsilon' = \varepsilon_\infty + A\sin(p\pi/2)\omega^{p-1} + B\sin(n\pi/2)\omega^{n-1} \qquad [3]$$

and the real part of the conductivity is:

$$\sigma = \sigma_0 + A\cos(p\pi/2)\omega^p + B\cos(n\pi/2)\omega^n. \qquad [4]$$

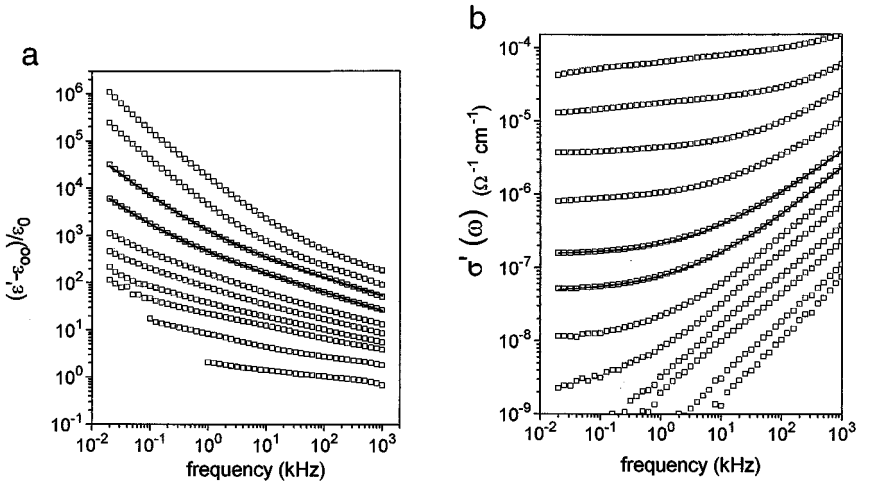

FIG. 3. (a) Real part of the relative permittivity calculated as $(\varepsilon' - \varepsilon_\infty)/\varepsilon_0$ as a function of frequency for the following temperatures in ascending order: 174, 227, 281, 313, 358, 394, 449, 491, 537, and 583 K. Lines in the figure are fits to expression $\varepsilon' = \varepsilon_\infty + A\sin(p\pi/2)\omega^{p-1} + B\sin(n\pi/2)\omega^{n-1}$ at 449 and 491 K. The high frequency permittivity value ε_∞ has been subtracted from the total permittivity ε' in order to remark the two different power law regimes at low and high frequencies. Na content of the sample was 0.675. (b) Real part of the conductivity as a function of frequency for the following temperatures in ascending order: 174, 193, 227, 249, 281, 313, 358, 394, 449, 491, 537, and 583 K. Lines in the figure are fits to expression $\sigma = \sigma_0 + B\cos(n\pi/2)\omega^n$ at 358 and 394 K. Na content of the sample was 0.675.

Lines in Figs. 3a and 3b are fits to Eqs. [3] and [4], respectively. Although permittivity representation (ε^*) is frequently used to describe dielectric phenomena while the conductivity representation ($\sigma^* = j\omega\varepsilon^*$) is preferred when dealing with charge dominated systems, we have chosen a mixed permittivity–conductivity representation to present complex admittance data. Some features appearing in the case of ionic conductors make a mixed representation more adequate. First, the increase observed in the real part of the permittivity at low frequencies is obscured in the conductivity representation. Observe that while the permittivity follows a great slope power law (ω^{p-1}, with p close to zero), the conductivity departs slightly from true dc behavior (σ is proportional to ω^p). On the other hand, the real part of the conductivity (calculated as $\omega\varepsilon''$) represents better the departures from pure nondispersive dc behavior at high frequencies.

The increase of the real part of the permittivity at low frequencies (see Fig. 3a) has frequently been observed in carrier dominated systems and is termed anomalous low frequency dispersion (ALFD). It is not clear whether the ALFD is an intrinsic regime (10) or is due to the blocking of charge carriers at internal boundaries. However for polycrystalline samples it is most likely due to the blocking at grain boundaries. Moreover, the permittivity data obtained at the highest temperatures (see Fig. 3a) show traces of saturation, which is characteristic of blocking phenomena. The ALFD is only observed at high temperature ($T > 450$ K), since the enhanced mobility allows ions to reach grain boundaries and accumulate there, giving rise to the observed increase of the capacitance.

One can observe in Fig. 3b that the real part of the conductivity is essentially nondispersive at low frequencies, but at high frequencies there is a temperature crossover to a power law regime of the ω^n. The conductivity behaves basically as:

$$\sigma = \sigma_0 + B\cos(n\pi/2)\omega^n. \qquad [5]$$

This expression is justified in view of Eq. [4] provided that the value of the exponent p is very close to zero in all cases. Departures from this behavior are observed only at high temperatures and low frequencies, where the conductivity shows a slight decrease toward low frequencies due to the above-mentioned blocking effects.

The ac power law regime of the conductivity at high frequencies has been widely observed in systems involving correlated hopping transport as for ionic conductors. In our case it seems to be due to ionic conduction. The fractional exponent n is a measure of the degree of correlation, i.e., n should be zero for random hopping and tends to one as the correlation increases.

All the samples analyzed show the same general trends of behavior explained above, but the value obtained for the exponent n varies with the Na content. Figure 4 shows data for various samples of the real part of the conductivity at several temperatures. For clarity, data sets corresponding to different Na contents have been vertically displaced. The temperature range for each set has been chosen to get a well developed power law at high frequencies. A linear fit to that portion is also marked in the figure to stress the decrease of the exponent n when Na is extracted. Higher n values for

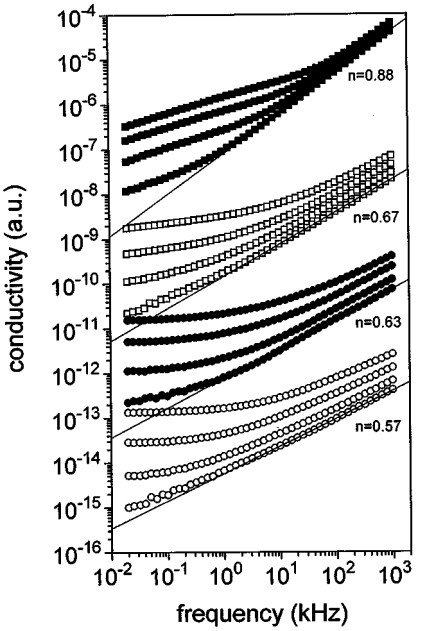

FIG. 4. Real part of the conductivity as a function of frequency for samples with different Na content: $\delta = 0$ (■) at temperatures 345, 389, 421, and 445 K; $\delta = 0.03$ (□) at temperatures 299, 337, 375, and 414 K; $\delta = 0.2$ (●) at temperatures 281, 313, 358, and 394 K; and $\delta = 0.4$ (○) at temperatures 212, 233, 250, and 264 K. Plots have been vertically displaced for clarity, preserving the scale for each sample.

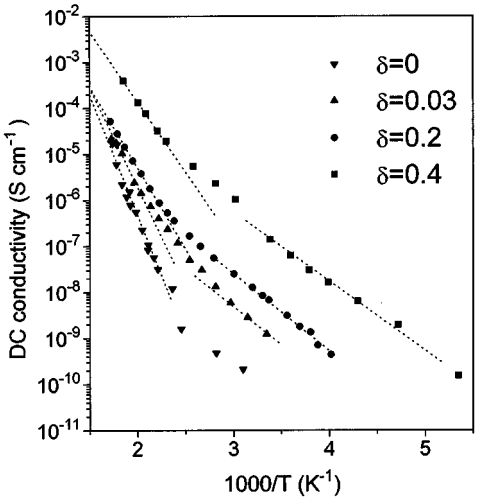

FIG. 5. DC conductivity as a function of temperature for samples with different Na contents. Down triangles correspond to the parent compound with a Na molar ratio of 0.875 per formula. Extracted samples (triangles correspond to 0.845, circles 0.675, and squares 0.475) show two activation energies.

Na-richer samples point to stronger correlation effects in ion motion. It has been proposed that these correlation effects in the hopping conduction mechanism occur because ions may backhop to their previous position after a hopping event, depending on their mutual interactions (11). The forward-backward sequences within a given time interval θ do not contribute to the measured conductivity at a frequency lower than $1/\theta$ and can be considered unsuccessful hops in this time scale. Higher n values mean higher probability of backhopping. It seems reasonable that for a higher concentration of Na ions the probability of a backhop increases.

The dc conductivity data fitting Eq. [5] has been plotted on Fig. 5 in an Arrhenius fashion. Two different slopes can be observed for low ($T < 450$ K) and high ($T > 450$ K) temperatures, respectively. The higher activation energy is most likely due to Na ionic conductivity. This conclusion is supported by the presence of blocking phenomena, which cause the increase observed in the permittivity at low frequencies or tilted spurs in complex impedance plots.

The observed increase in conductivity after sodium extraction seems to indicate that the increase in mobility more than compensates for a decrease in the number of carriers. The ionic conductivity of Na is proportional to the ion concentration and their mobility, while Na mobility is proportional to the number of vacant sites where a Na ion can hop. This combined effect explains the higher conductivity obtained for the samples with lower Na content (see Fig. 5). On the other hand, some authors have proposed that correlation effects may increase the activation energy of the dc conductivity. The activation energies of the ionic conductivity obtained for the different samples are collected in Table 1 together with values of the exponent n. The higher activation energy for a higher Na content in the samples probably results from the reduced number of vacancies, which favors mutual interactions among charge carriers.

It is opportune to recall here some structural features of the parent compound. Each sodium atom has a nonregular prismatic environment of six nearest-oxygen atoms. Three additional oxygen atoms are located out of the rectangular faces of the prism (Fig. 6a). Therefore, the polyhedron can be regarded as a distorted tricapped trigonal prism (*ttp*) of oxygen atoms with the sodium atom in the center. The prisms share their triangular faces, which are formed by the oxygen atoms O2–O3–O4, along the double tunnel. We wish to address here some structural changes related to the Na–O polyhedron on sodium removal. Single crystal

TABLE 1
Activation Energies and *n* Parameter for Varying Na Contents

Na molar content	E_1	E_2	n
0.875	1.1	—	0.88
0.845	0.85	0.35	0.67
0.675	0.7	0.34	0.63
0.475	0.58	0.30	0.57

structural refinements showed that the basic framework undergoes a slight rearrangement (8). A consequence of the relaxation of the framework structure is a significant change in interatomic distances. The main Na–O and O–O distances of the *ttp* for a nonoxidized ($\delta = 0$) and an oxidized ($\delta = 0.30$) single crystal are listed in Table 2. The average Na–O distance increases by 0.02 Å (from 2.74 to 2.76 Å), whereas the distances between the three above-mentioned oxygen atoms, which constitute the triangular prism face, increase (Fig. 5). To hop from one determined site to a neighboring vacant site along the tunnel, each sodium atom has to go through such a triangular O2–O3–O4 "oxygen window". Obviously, the tunnel "opens" on sodium extraction; better sodium ion mobility is also expected in the samples with lower sodium content from a structural point of view.

The lower activation energy regime deserves a more careful discussion since, as blocking effects are not observed, the electronic or ionic nature of the conductivity cannot be ascertained from complex admittance measurements alone.

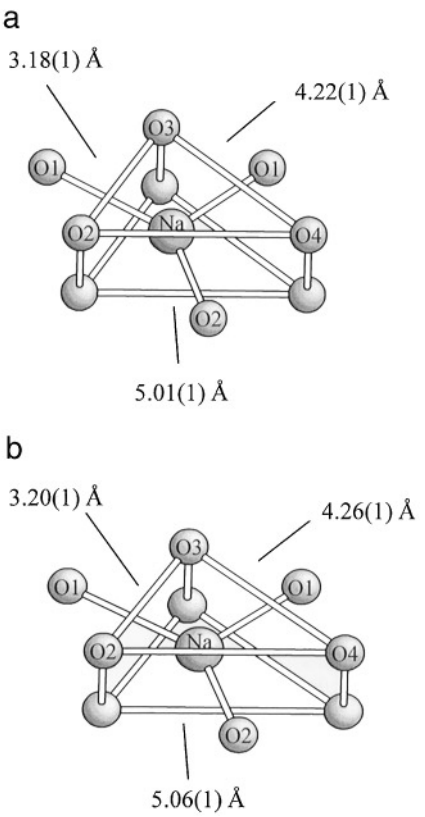

FIG. 6. Perspective view of the tricapped trigonal prism formed by oxygen atoms with the sodium atom in the center (a) before and (b) after sodium extraction. The "opening" of the triangular faces (O2–O3–O4, thick lines) can be readily deduced from the change in interatomic distances (after Ref. (8)).

TABLE 2

Important Interatomic Distances (Å) in $Na_{x-\delta}Fe_xTi_{2-x}O_4$ ($\delta = 0$ and 0.30) after Ref. [8] (estimated standard deviations are given in parentheses)

Crystal	$\delta = 0$	$\delta = 0.30$
	Na–O polyhedron	
Na–O1 (1×)	3.15(1)	3.21(2)
–O2 (2×)	2.29(1)	2.26(2)
–O2′ (1×)	2.598(9)	2.61(1)
–O3 (2×)	2.398(8)	2.45(1)
–O1′ (1×)	2.64(1)	2.69(2)
–O4 (2×)	3.474(9)	3.47(1)
average Na–O	2.74	2.76
O1–O2	2.891(9)	2.87(1)
O1–O3	2.923(9)	2.91(1)
O1′–O3	2.778(8)	2.80(1)
O1′–O4	2.980(8)	2.97(1)
O2–O2	3.483(9)	3.55(1)
O2–O3	3.18(1)	3.20(1)
O2–O4	5.01(1)	5.06(1)
O2′–O4	2.933(9)	2.94(1)
O3–O4	4.22(1)	4.26(1)
average O–O[a]	2.99	2.99
average O–O[b]	4.13	4.17
	$(Fe,Ti)O_6$ octahedron	
(Fe,Ti)1–(Fe,Ti)1 (Fe,Ti)2–(Fe,Ti)2	2.968(1)	2.942(1)

[a] Includes all distances of neighboring oxygen atoms in the *ttp* polyhedron.

[b] Refers to the distances between oxygen atoms O2–O3–O4 of the triangular window (see text).

Concerning the lower activation energy obtained for low temperatures, no clear traces of blocking were observed in conductivity plots, possibly due to an electronic contribution to the total dc conductivity.

As discussed above, the extraction process involves substantial changes in the interatomic distances: The shortest distance between Fe and Ti atoms is found along the "rutile-like" tunnel direction. This metal–metal distance decreases from 2.968(2) Å ($\delta = 0$) to 2.942(1) Å for $\delta = 0.30$ (Table 2). This shortening, due to the smaller size of Fe^{4+} with respect to Fe^{3+} and the related increase in covalency of the metal–oxygen bond, might be enough to produce some overlapping between Fe d orbitals, giving rise to electronic conduction. The observed metal–metal distance in the oxidized sample ($\delta = 0.30$) is very close to the limiting distance for direct metal–metal overlap in the rutile structure, which has been estimated by Goodenough as 2.93 Å (11). In contrast to the oxidized samples, the starting material, $Na_{0.875}Fe_{0.875}Ti_{1.125}O_4$, shows an electronic absorption spectrum typical of a spin-free d^5 ion with all electrons localized in an octahedral oxygen environment (Fig. 7,

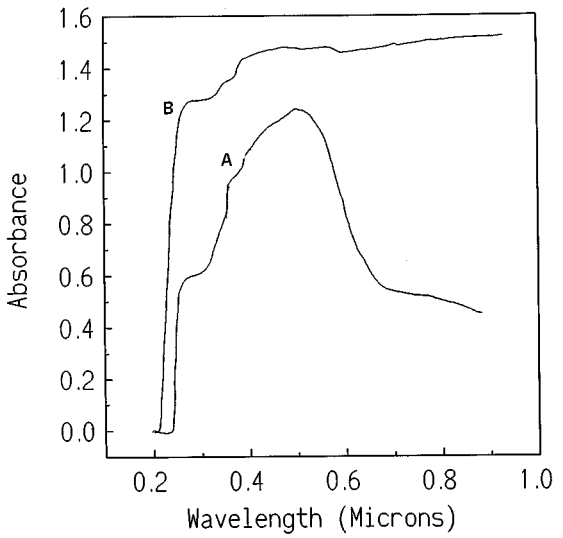

FIG. 7. Electronic absorption spectra of the starting material (A) and an oxidized sample with $\delta = 0.20$ (B) in the wavelength range 900–200 nm.

curve A). On the other hand, significant UV absorption, characteristic of free electrons, is observed for these oxidized black samples down to the IR range (Fig. 7, curve B).

In this context, we would like to remark that the diffusion of lithium in rutile (13) was found to be strongly anisotropic, and the diffusion coefficient D perpendicular to the tunnel *c*-axis was smaller than D parallel by a factor of 10^8! Therefore, the perpendicular motion of sodium atoms, bigger in size than lithium, with crossing to a neighboring tunnel through an oxygen wall in the parent rutile-related compound, as well as in rutile itself, would be still more hindered. On the basis of this result, we should exclude the possibility of a skew motion mechanism in the bigger sodium atoms perpendicular to the tunnel.

ACKNOWLEDGMENTS

We thank CICYT (MAT 95/0809) and Universidad San Pablo – CEU (USP 5/96 and 8/97) for financial support. The DAAD is also acknowledged for providing a fellowship to A.K.

We are also grateful to A. Santos (Instituto de Materiales de Madrid, C.S.I.C.) for performing the UV/VIS spectra.

REFERENCES

1. M. J. Sienko and T. N. Truong, *J. Am. Chem. Soc.* **83,** 3939 (1961).
2. A. Várez, C. León, J. Santamaría, J. M. Rojo, J. Sanz, E. Morán, F. Sánchez-Quesada, and M. A. Alario-Franco, *J. Phys.: Condens. Matter* **7,** 5477 (1995).
3. B. F. Decker and J. S. Kasper, *Acta Crystallogr.* **10,** 332 (1957).
4. A. F. Reid, H. K. Perkins, and M. J. Sienko, *Inorg. Chem.* **7,** 119 (1968).
5. W. G. Mumme and A. F. Reid, *Acta Crystallogr. Sect. B* **24,** 625 (1968).
6. A. F. Reid, *Inorg. Chem.* **6,** 631 (1967).
7. A. Kuhn, N. Menéndez, F. García-Alvarado, E. Morán, J. D. Tornero, M. A. Alario-Franco, *J. Solid State Chem.* **130,** 184 (1997).
8. A. Kuhn, F. García-Alvarado, E. Morán, and M. A. Alario-Franco, *Solid State Ionics* **86–88,** 811 (1996).
9. A. K. Jonscher, *in* "Dielectric Relaxation in Solids." Chelsea Dielectric Press, London, 1983.
10. L. A. Dissado and R. M. Hill, *J. Chem. Soc., Faraday Trans.* **80,** 291 (1984).
11. K. Funke, *Prog. Solid St. Chem.* **22,** 111 (1993).
12. J. B. Goodenough, *in* "Magnetism and the Chemical Bond." Interscience Publisher Inc., New York, 1963.
13. O. W. Johnson, *Phys. Rev. A* **284,** 136 (1964).